Singular spectrum and principal component analysis of soil radon (Rn-222) emanation for better detection and correlation of seismic induced anomalies

Timangshu Chetia[1, 2], Saurabh Baruah[1], Chandan Dey[1, 2], Sangeeta Sharma[1], Santanu Baruah[1]

[1]Geoscience & Technology Division, CSIR-North East Institute of Science and Technology (CSIR-NEIST), Jorhat-785006, Assam, India
[2]Academy of Scientific and Innovative Research (CSIR-NEIST), Jorhat-785006, Assam, India

[*]*Correspondence to*: Santanu Baruah (santanub27@gmail.com)

Abstact. In the recent years there are several reporting's of anomalous seismic induced temporal changes in soil radon emanation. It is however well known that radon anomalies apart from seismic activity are also governed and controlled by meteorological parameters. This is the major complication which arise for isolating the seismic induced precursory signals. Here in the investigation the soil radon emanations temporal variability at Multiparametric Geophysical Observatory (MPGO), Tezpur, is scrutinized in the lime light of singular spectrum analysis (SSA). Further prior applying SSA Digital filter (Butterworth low pass) is applied to remove the high frequen.o9cy quasi periodic component in the time series of soil radon emanation. It was scrutinized that sum of just 9 eigenfunctions were sufficient enough for reproducing the prominent characteristics of the overall variation. This perhaps also evinces that more significantly produced fluctuations are mostly free from natural variations. The variations in soil temperature was observed to be dominated by daily variations similar to radon variation which account to 97.99 % whereas soil pressure accounts for 100 % of the total variance which suggests that daily variations of soil radon (Rn-222) emanation are controlled by soil pressure in MPGO, Tezpur during the investigation period followed by soil temperature. The study concludes that SSA eliminates diurnal and semidiurnal components from time series of soil radon emanation for better correlation of soil radon emanation with earthquakes.

1 Introduction

Radon (Rn-222) is a noble gas, a decay product of radium with atomic number, Z=86 and a half-life of nearly 3.8 days. Because of its short decay time, amount changes in its production from the rock is quite evidenced. Ulomov and Mavashev in the year 1971 (Ulomov and Mavashev, 1971) first suggested the correlation of radon concentration with earthquakes. It has been scrutinized that the radon concentration has correlation to earthquakes and volcanic eruptions (Walia et al., 2005; Singh et al., 2010; Chetia et al., 2019). Significant radon concentration anomalies were also observed prior to the Uttarkashi earthquake of 20th October, 1991; m_b~6.5 (Virk and Singh, 1994). Radon concentrations was monitored in the North West Himalaya for earthquake prediction studies and empirical equation between earthquake magnitude, epicentral distance and precursory time were examined (Choubey et al. 2009). Earthquake prediction depending entirely on precursory phenomena is empirical and comprises many applied problems. Among various geophysical parameters soil radon is preferred and used for earthquake precursory studies because of its ease of detectability. Radon in nature has different isotopes: Rn-222 (half-life~3.8 days), Rn-220 (Thoron, half-life~54.5 s) and Rn-219 (half-life~3.92 s). The utmost prominent is Rn-222 because of its longer half-life which is a product of Ra-226 decay process. The Rn-222 emanates from soil or crust either by diffusion or convection and reaches the atmosphere. The soil radon emanation concentration is generally assigned to developments of micro-cracks, fissure and fracture due to dilatancy prior to earthquake. This process enhances the transportation of Radon from its original enclosure following the cracks into the atmosphere. Variations of soil radon and thoron concentrations were also observed in fault zone prior to earthquakes SW Taiwan. Anomalous peaks were discernible usually few days or weeks prior to the earthquakes (Yang et al., 2005).

North-East India (NE India) is highly vulnerable to earthquake and lies in seismic zone V (BIS 2002) and frequent occurrence of earthquake facilitates the probability of finding

precursory phenomena which may lead to a successful prediction in near future. The estimated cumulative probabilities show about a similar recurrence period of about 15-25 years from the occurrence of last earthquake for a forecast of large earthquakes (Mw > 5) in the NE-India region and its vicinity (Chetia et al., 2019). With this objective a Multiparametric Geophysical Observatory (MPGO) in Ouguri Hills (Latitude N26.61^{o}; Longitude E92.78^{o}, Elevation~82m), Tezpur, Assam, India with the installation of several geophysical instruments collecting data simultaneously, portray an opportunity towards identification of precursory signatures prior to earthquakes. Earthquake precursory and prediction studies advanced in late 1970s and Heicheng earthquake of 4th February is a land- mark which was in short-term successfully predicted in 1975 in China (Adams, 1976). The accomplished medium term forecast of M~7.5 earthquake on 6th August, 1988 in northeast Indian region (Gupta, 1988) encouraged to strengthen such studies in India. Another successful short term prediction was done of ($M \geqslant 4$) in Koyna region of western India, famous for Reservoir Triggered Seismicity (Verma and Bansal, 2012).

The study tries to correlate radon emanation in soil gas with earthquakes within the epicentral distance of 100 km of mb > 3.1 from MPGO, Tezpur which is situated in a highly tectonically strained and seismically active region. The reason for considering the criteria of 100 km with mb > 3.1 is the tectonic setting of the study area which is bounded by two major fault namely Kopili and the Bomdila Faults. The region is highly stressed because of geotectonic settings where earthquake do occur periodically within very short span of time. Kopili fault zone is experiencing compressional stress due to the Indo-Burma arc and Himalyan arc to the east and the north respectively which is characterized by transverse tectonics. The Bomdila Fault inter-weaves across three major tectonic domains of the NE-India, namely MCT, MBT and Naga-Disang thrust along NW-SE direction. (Kayal, 2010). The empirical relation for the energy release E to the magnitude (Gutenberg, 1956) gives $E > 10^{9.2}$ for

earthquake of mb > 3.1. Stress and strain are directly proportional and hence in order to obtain adequate stress build up processes for observing precursory signals in temporal soil Radon emanation the criteria of 100 Km with mb>3.1 is taken into consideration. The major problem is the removal of quasi periodic, diurnal (mostly due to temperature) and semidiurnal (mostly due to pressure) components (Kumar et al., 2015). Radon anomalies are governed by seismic activity as well as by meteorological parameters (soil temperature, pressure, rainfall, moisture and even wind for atmospheric radon (Stranden et al., 1984; Choubey et al., 2009; Walia et al., 2005) which in turn makes it more complex for identifying the seismic induced anomalies. Here in the investigation characteristics features of temporal soil radon concentrations variability at MPGO, Tezpur is scrutinized by applying singular spectrum analysis (SSA) in concern to the objective of filtering the meteorological parameters on radon concentration. SSA is a relatively innovative and powerful advanced method which has been used across many applied problems for different scientific fields (e.g. Fraedrich, 1986; Serita et al., 2005). Seismic induced emanation of soil gas radon is a complex phenomenon to be studies based on mathematical, statistical analysis and modellings. Nonlinear methods such as power spectrum, fractal-multifractal analysis and singular spectrum analysis etc. probably are commanding tools which reveals the nonlinear features and mechanism of soil gas radon emanation processes. The major advantages of Caterpillar-SSA method is that it does not require better understanding of time series parametric model and extensively applicable to varied spectrum of diverse temporal data. It can also be applied to match with non-stationary temporal data and also permits to estimate structures even for short temporal data. Here Caterpillar-SSA method is used to study the temporal soil gas radon and the foremost concept of SSA is applying PCA on trajectory matrix acquired from the original time series following time series reconstruction.

2 Seismotectonics of the region

In middle of the active Kopili and Bomdila fault, the MPGO is situated. The Kopili and Bomdila faults comprise Neogene-Quaternary sediments, which directly were deposited over the Archean basement. The Kopili fault zone in an approx is 100 km in width and 300 km in length. It is a NW-SE trending strike-slip fault (Kayal et al., 2006, Bhattacharya et al., 2008, 2010). The two Precambrian massifs - the Shillong Plateau and the Mikir Hills is delineated by the tectonic disposition of the Kopili fault. MPGO is bounded to the north by the Main Boundary Thrust (MBT) and to the south by the NE-SW trending Belt of Schuppen (Figure 1). The Bomdila fault is strike slip fault of about 400 km in length which trends along WNW-ESE direction. The northern portion of the fault mostly lies in the Gondwana, Paleogene and Neogene sediments. This fault is surrounded by the Belt of Schuppen to the east and south by the Mikir massif and to the west. The fault cuts across the Himalayan fold belt towards the north (Nandy and Dasgupta, 1991).

The Kopili Fault has produced two large earthquakes (Figure 1) M_w~7.7, 1869 event (Figure 1) in the south eastern edge of the fault contravening the Naga-Disang thrust and M_w~7.2, 1943 earthquake which occurred farther to the north of 1869 event within a period of nearly 75 years (Kayal, 2008). It is highly active with strong seismicity discernible down up to depth of about 50 km, and which extends to the Main Central Thrust (MCT) in the Bhutan Himalaya. Even if MCT is dormant (Ni and Barazangi, 1984), intense activity is observed at the region where Kopili Fault meets the MBT and MCT (Nandy, 2001; Kayal et al., 2010, 2012). This is demonstrated by the August 19, 2009 Earthquake (M_w~5.1) in the Assam Valley that occurred in the center of the Kopili fault zone and the September 21, 2009 strong Bhutan Himalaya earthquake (M_w~6.3) that occurred at the northern end of the Kopili fault where it connects with the MCT (Kayal et al., 2012). Both the earthquakes are shallow focus (depth ~ 10 km) showing right lateral strike-slip faulting (Kayal et al., 2010) which suggests that the Kopili fault zone is experiencing compressional stress due to the Indo-Burma arc and Himalyan

arc to the east and the north respectively which is characterized by transverse tectonics. The Bomdila Fault inter-weaves across three major tectonic domains of the NE-India, namely MCT, MBT and Naga-Disang thrust along NW-SE direction. The earthquake events along Bomdila fault occur in a diffused pattern having post-collisional intracratonic characteristics (Nandy and Dasgupta, 1991). It is observed that, the Upper Brahmaputra Valley stretching between the Bomdila Fault and almost near NW-trending Mishmi Thrust in the northeast is seismically dormant, and is recognized as the Assam Gap (Khattri, 1983).

3 Method and techniques

3.1 Soil radon (Rn-222) time series

A BMC2 barasol manufactured by Algade is into operation for soil radon emanation time series data in MPGO for earthquake prediction and precursory studies. Soil gas radon emanation every 15 minutes is being continuously monitored. The barasol probe is kept fitted inside a plastic tube (length 1.5m and diameter of 0.0635m) with open bottom dug inside the ground in such a way that the detection unit (detector sensitivity-0.02 pulses/h for 1 Bq/m^3 and saturation volumetric activity-3MBq/ m^3) which is at the bottom of the probe lies 1m from the ground level. A silicon alpha detector detects the radon gas which enters the detection chamber when it emanates from the soil. The radon pass in a detection volume over three cellulose filters which allows to trap all the solid daughter products of radon. The sensor is a fixed silicon detector with a depleted depth of 100μm and 400 mm^2 of sensitive area. It performs the counting by atomic spectrometry of radon (Rn-222) and daughter products created in the detection volume (with window customized between 1.5 MeV and 6 MeV). The probe system is embedded with soil pressure and temperature sensor. The sensor calibration permits the volumic activity of the radon (Rn-222) to be evaluated. In the present investigation the soil radon emanation temporal variability at MPGO, Tezpur the radon data were prudently checked

for no gaps or discontinuous jump. Digital filter (Butterworth) is applied to eliminate the high frequency quasi periodic components form the soil radon time series for better discernibility of seismic induced anomalies.

3.2 Singular Spectrum Analysis

The SSA results and graphs in the investigation are acquired by using Caterpillar-SSA 3.40 software (Alexandrov and Golyandina, 2004). Window selection rule applied to the time series is one half of the length of the time series to meet the theoretical requirements for the investigation (Golyandina, 2010, Khan, 2011, Hassani, 2007). The singular value decomposition (SVD) alogorithm was applied as it is more accurate than QR iteration which are the most common algorithm for solving of eigenvalues and singular value problems (Demmel and Veselić, 1992). The main objective of SSA is decomposing the original time series into sum of series such that each of the component in this sum can be known (either as a trend, periodic or quasi-periodic components) or noise. This is accomplished by decomposition and reconstruction. At the first the time series is decomposed following the reconstruction of the original time series (which is without noise). The methodology adopted here is first to embedding a 1-dimension time series say, $Y_T = (y_1,...,y_T)$ into a multi-dimensional time series $X_1,...,X_K$ having vectors $X_i = (y_i,...,y_{i+L-1}) \in R^L$ (Golyandina et al., 2001, 2001). Here the value of $K = T - L + 1$. The X_i Vectors are called L-lagged vectors. The embedding depends on the window length L, such that $2 \leq L \leq T$ which results for trajectory matrix (Hankel matrix: diagonal elements $i + j$ = const. are equal) $X = [X_1,...,X_K]=(X_{ij})_{i,j=1}^{L,K}$. Secondly the Singular Value Decomposition (SVD) of the trajectory matrix is performed to represent it as an addition of bi-orthogonal elementary matrices having rank one. Represented by $\lambda_1,...,\lambda_L$ which are the Eigen-values of XX' in a descending order of magnitude ($\lambda_1 \geq ...\lambda_L \geq 0$) and by $U_1,...,U_L$ which are the orthonormal system (i.e. (Ui, Uj) =0 for $i \neq j$) is the orthogonality property and $||U_i||$=1,

of the eigenvectors of the matrix XX' corresponding to these eigenvalues. (U_i, U_j) is the inner product of the vectors U_i and U_j and $||U_i||$is the norm of the vector U_i. The Set

$$d = \max (i, \text{ such that } \lambda_i > 0) = rank\ X \quad \text{(I)}$$

If we represent V_i = X' $U_i/ \sqrt{\lambda_i}$, then SVD of the trajectory matrix can be represented as:

$$X = X_1 + \cdots + X_d \quad \text{(II)}$$

Here $X_i = \sqrt{\lambda_i} U_i V_i'$ ($i = 1,...,d$).

Thirdly the series reconstruction is accomplished by grouping, to split the elementary matrices (X_i) into various groups and addition of the matrices within each and every group. The splitting of the elementary matrices Xi into several groups and summation of the matrices within individual group is grouping. Say $I = (i_1, \ldots, i_p)$ is a group of indices $i_1, \ldots, i_p$. Now for the group I of corresponding matrix X_I is defined as $X_I = X_{i1} + \cdots\cdots + X_{ip}$. The spilting of the of the set with indices $J = 1,\ldots, d$ on the disjoint subsets $I_1,..., I_m$ resembles to the illustration

$$X = X_{I_1} + \cdots + X_{Im}. \quad \text{(III)}$$

This procedure of selecting the sets $I_1,\ldots, I_m$ is termed as eigentriple grouping. For given group I the contribution of the component X_I into $X_{I1} + \cdots + X_{Im}$ is estimated to the corresponding eigenvalues as: $\sum_{i \in I} \lambda i \,/\, \sum_{i=1}^{d} \lambda i$.

Finally diagonally averaging transfers each I matrix into a time series, which is an additive component of the initial series Y_T. If z_{ij} is an element of the matrix Z. Then k-th term of the produced series is acquired by averaging z_{ij} for i, j such that $i + j = k + 2$. This procedure is known as diagonal averaging (Hankelization) of the matrix Z. The Hankelization of a matrix

196 Z is the Hankel matrix HZ which is the trajectory matrix corresponding to the series obtained
197 from diagonal averaging. Hankelization is a best logical technique that HZ matrix is the nearest
198 to Z among all corresponding size of Hankel matrices (Golyandina et al., 2001). Now applying
199 the Hankelization technique to each and every matrix components in equation III, we get

200 $$X = \tilde{X}_{I_1} + \ldots + \tilde{X}_{I_m} \quad \text{(IV)}$$

201 Here $X_{I_1} = HX$ corresponding to initial series $Y_T = (y_1, \ldots, y_T)$ decomposition into a
202 sum of m series as

203 $$y_t = \sum_{k=1}^{m} \tilde{y_t^{(k)}} \quad \text{(V)}$$

204 Here $\tilde{y_t^{(k)}} = \tilde{y_1^{(k)}} + \ldots + \tilde{y_T^{(k)}}$ corresponds matrix X_{1j}.

205 Covariance matrix is a matrix of covariances between the values $X(t)$ and $X(t+k)$., where
206 k is a lag. When k is positive $X(t)$ and $X(t+k)$ tends to fluctuate together. The covariances among
207 $X(t)$ and X$(t+k)$ can be estimated as

208 $$\text{COV} = \frac{\sum_{i=1}^{n} (X(t) - \overline{x(t)})(X(t+k) - \overline{x(t+k)})}{n-1} \quad \text{(VI)}$$

209 Where $\overline{x(t)}$ and $\overline{x(t+k)}$ represents the mean of $x(t)$ and $x(t+k)$ correspondingly.
210 Now covariance matrix ($\tilde{C}$) can be obtained by putting equal values $\tilde{c}_{ij}$ at each matrix
211 antidiagona $|i - j| = k$ as

212 $$\tilde{c}_{ij} = \frac{1}{N-|i-j|} \sum_{m=1}^{N-|i-j|} x_m \, x_{m+|i-j|} \quad \text{(VII)}$$

213 Where $1 \leq i, j \leq L$, N is the length of the time series and $|i - j| = k$.

214 From the eigenvectors of the covariance matrix measured at different lags the principal
215 components of the time series is estimated. The principal components is also a time series

having same length as the "embedded" time series. The computation of principal component is from simple matrix product as

$$PC = \tilde{C} * \text{matrix of eigenvectors} \quad \text{(VIII)}$$

Where $\tilde{C}$ is the covariance matrix, whose elements are $\tilde{c}_{ij}$.

The exemplification of how discretely different component can be separated from each other is based on studying the SSA properties. To successfully decompose (SSA) the series Y_T the subsequent additive components of the series should be almost separable from each other. The weighted correlation is also known as w-*correlation* which is the natural measurement of dependencies among two series Y_T^1 and Y_T^2 given as:

$$\rho_{12}^{\omega} = \frac{(Y_T^1, Y_T^2)_{\omega}}{\left||Y_T^1|\right|_{\omega}\left||Y_T^2|\right|_{\omega}} \quad \text{(IX)}$$

Here, $\left||Y_T^1|\right|_{\omega} = \sqrt{(Y_T^i, Y_T^i)_{\omega}}$, $(Y_T^i, Y_T^j)_{\omega} = \sum_{k=1}^{T} \omega_k y_k^i y_k^j$, $(i, j = 1, 2)$, $\omega_k = \min\{k, L, T-k\}$ while assuming $L \leq = T/2$.

If the absolute value of w-correlations is small, the corresponding series are almost *w*-orthogonal. On the other hand if it is large, the series are not *w*-orthogonal and are considered probably un-separable. If the reconstructed components exhibit *w*-correlation zero, it signifies the two components to be separable. Large values of w-correlations between reconstructed components indicate that the components should possibly be gathered into one group and correspond to the same component in SSA decomposition (Hassani, 2007).

4 Results

The average value of radon for a period of six month from April 2017-September 2017 was found to be in the range 55-117 kBq/m^3. The average emanation of soil-gas radon and the

standard deviation at MPGO from April to September 2017 is illustrated in Table 1. Simultaneously variation of soil temperature and pressure with radon emanation was observed. Usually, radon shows positive correlation with temperature i.e. the soil radon concentration increases with increase in temperature and decreases as temperature decrease. The correlation coefficient (Pearson correlation) between radon and temperature is found to be 0.5 signifying positive correlation, while the correlation coefficient between radon and pressure is found to be -0.5 signifying negative correlation with an average temperature and pressure of 28.60 ^{0}C and 991.03 mbar respectively during afore mentioned period. The positive correlation of radon with temperature might be due to the rise in diffusion rate with temperature (Sharma et al. 2000; Singh et al. 2008). The negative correlation coefficient was found for soil radon and pressure which signify, with the increase in pressure, the radon emanation decreases while with the decrease in pressure the radon emanation increases. In general, the negative correlation is due to the diffusion process which slows down with increase in pressure, which in turn decreases the radon concentration in the soil. The average value of pressure, temperature, standard deviation, coefficient of variation and correlation coefficient for the observation period is detailed in Table 2. The maximum and minimum temperature observed was 31.24 ^{0}C and 23.78 ^{0}C i.e. a change of 7.46 ^{0}C during the period of observation. Simultaneously, the maximum and minimum pressure during the period of observation was 999.32 mbar and 980.72 mbar i.e. a change of 18.6 mbar. Digital filter (Butterworth) is applied to eliminate the high frequency quasi periodic components from the soil radon time series for better discernibility of seismic induced anomalies and is represented in Figure 2.

The covariance matrix of the first 9 group of soil radon (Rn-222) time series is represented in Figure 3.The singular value decomposition (SVD) to Rn-222 data evinced that first 9 eigenfunctions (Figure 4) when grouped resulted for 99.90 % of the total variance in the individual time series. The eigenfuction group 1 and 2 represents the aperiodic component and

group 3 to 9 represented periodic components. It has been earlier studied that the periodic components of radon data extracted by SSA consisted of diurnal and semidiurnal components since the components included variation of 24-hour and 12- hour period (Kumar et al., 2015). The decomposed eigenvectors in soil radon time series is grouped into two classes as diurnal and semidiurnal variation. The sum of eigenfuction group 1 and 2 accounts for 98.62 % and group 3 to 9 accounts for 0.48 % of the variance. Radon variations is governed by daily variations, which accounts to 99.90 % of the total variance in soil gas radon at the MPGO, Tezpur. The Principal Component of soil radon (Rn-222) related to the first 9 grouping of eigentriples is represented in Figure 5 and w-correlation matrix for the 9 reconstructed components is represented in Figure 6.

The covariance matrix of the first 9 group of soil temperature and pressure time series is represented in Figure 7 and Figure 11 respectively. The decomposed eigenfunctions for soil temperature and pressure time series by applying SSA is represented in Figure 8 and Figure 12 respectively. The first 9 eigenfunction group from SVD to atmospheric temperature records accounts nearly about 99.99 % and first 9 eigenfunction group of soil pressure 100 % of the variation respectively. It is discernible that first eigenfunction 1 alone itself is capable of producing 100 % variation but the time series is well modeled when first 9 eigenfunction is grouped. This evinces SVD to radon, soil temperature and soil pressure data evince that first 9 eigenfunction accounts >98.00 % of the variance of the individual data series. This is fascinating to observe that sum of first 9 eigenfunction is fairly sufficient to reproduce the prominent features of the overall variation. This also suggests that the most significantly produced variations are mostly free from naturally induced variations. Soil pressure variations are dominated by semidiurnal variations by 100 % of the total variation in atmospheric pressure at MPGO, Tezpur. On the other hand soil temperature variations is dominated by daily variations like radon variation which account to 97.99 % whereas soil pressure accounts for

100 % of the total variance. This suggest that daily variations of soil radon (Rn-222) emanation are controlled by soil pressure in MPGO, Tezpur during the investigation period followed by soil temperature. The Principal Component of soil temperature related to the first 9 grouping of eigentriples is represented in Figure 9 and w-correlation matrix for the 9 reconstructed components is represented in Figure 10. The Principal Component of soil pressure related to the first 9 grouping of eigentriples is represented in Figure 13 and w-correlation matrix for the 9 reconstructed components is represented in Figure 14. The reconstructed time series for soil radon (Rn-222), temperature and pressure is represented is Figure 15 and it's residual in Figure 16. It is also discernible that the during the investigation time period the pressure change was more than temperature change which also evinces the variation of soil radon at MPGO, Tezpur was more governed by pressure followed by temperature change. The quasi periodic, diurnal (periodic mostly due to temperature) and semidiurnal (aperiodic mostly due to pressure) were eliminated by Singular Spectrum Analysis in the reconstructed time series by grouping and analyzing the eigenfunctions and principle component of individual time series of Rn-222, temperature and pressure respectively. The soil pressure and temperature were found to be negatively correlated to each other (-0.62) which produces a pseudo effect in the soil radon time series. The grouping and reconstruction of the time series also eliminates these pseudo effect arising due soil pressure and temperature.

5 Discussion

The reconstructed soil radon time series along with the seismic activity during the investigation period is shown in Figure 17. The hypocentral parameters of the earthquake events found to have correlation with soil radon emanation is listed in Table 3. The earthquakes are selected from a catalogue which follow Stationary Poisson process where we have adopted declustering method by Reasenberg (Reasenberg, 1985). After declustering of the database, we have used the maximum likelihood algorithm provided by ZMAP (Wiemer, 2001) to perform

a Gutenberg-Richter regression (Gutenberg and Richter, 1944). Here, the magnitude range of earthquakes catalog indicate relatively high magnitude of completeness (MC~4.7) for the region. It was observed that there were certain positive amplitude rise anomalies in radon emanation prior to six out of 9 earthquakes which occurred in the vicinity (100 km radially from MPGO,Tezpur). Increase in the soil radon concentration is generally assigned to developments of microcracks, fractures and fissure caused by dilatancy prior to earthquake. This process enhances the transportation of radon from its original enclosure following the cracks. The rise in soil radon concentration prior to an earthquake may be due to the strain buildup processes in the area. During this process, very small fractures are developed in the rocks which enhances the contribution of radon gas to the soil near the surface of earth (Miklavčić et al., 2008). Three earthquake events were preceded by negative anomalies. The negative anomalies might be due to the circumstance that during the final stage of dilatency model prior to an earthquake the Rn-222 emanation can be stable or it can decrease (Tomer, 2016). This is because, during the final stage prior an earthquake, rupture occurs and fluid pressure and stress on rocks is released (Bakhmutov and Groza, 2008). The fluid pressure increases may result in water level rise (pore spaces probably gets filled by water and diffusion rate of radon is more in void than in water filled pore space; Nielson et al., 1984; Merolla et al., 2003) and this probably does not allow the soil gas Rn-222 to escape from the surface which in turn reduces or stabilizes the emanation of Rn-222. Further a decreasing radon anomaly as observed in this study may be the result of squeezing effect of compressional stress built up in the rock, which in turn result in soil porosity changes at micro scale. There were certain events which occurred on the same day or just a very short seismic gap of 1 or 2 days. Here in the case earthquake with higher magnitude might also be the probable reason for the anomalous behavior of the soil gas radon emanation, as for spatio-temporal clustered earthquakes, the largest magnitude earthquake is presumed to precede the anomalies in radon emanation

(Hartmann and Leavy, 2005). Positive as well as negative anomalies were observed prior to 9 events which occurred in the vicinity (100 km radially from MPGO) with in a short span of time.

6 Conclusion

The investigation concludes that digital filter assists in eliminating the high frequency quasi periodic components from the time series. The SSA method helps eliminating the diurnal and semidiurnal fluctuations from soil radon time series for improved correlating and detection of the soil radon emanation with seismic activity. The investigation also evinced that radon is dominated by daily variation at MPGO,Tezpur and is controlled by soil pressure followed by temperature. It is also concluded that principle component analysis helps in removing the pseudo effect pertaining to simultaneous soil pressure and temperature effect. It was observed that there were certain positive amplitude rise anomalies in radon emanation prior to six events out of 9 earthquakes which occurred in the vicinity (100 km radially from MPGO,Tezpur) within a short span of time. The increase of radon emanation with temperature might be the result of increasing diffusion rate with temperature. Three earthquake events were preceded by negative anomalies. The negative anomalies might be due to the circumstance that during the final stage of dilatency model prior to an earthquake the soil gas radon emanation can be stable or it can decrease. This is because, during the final stage prior an earthquake, rupture occurs and fluid pressure and stress on rocks is released. Further a decreasing radon anomaly as observed in this study may be the result of squeezing effect of compressional stress built up in rock, which in turn changes porosity of soil at micro scale.

Acknowledgements. We acknowledge our sincere thanks to Ministry of Earth Sciences (MoES) Government of India for providing funds vide project no.MoES/P.O.(Seismo)/NPEP-16/2011. We thank Director, CSIR-NEIST Jorhat for giving necessary permission to publish this paper.

References

Adams, R. D.: The Haicheng, China, earthquake of 4 February 1975; the first successfully predicted major earthquake, Earthquake Engineering & Structural Dynamics, 4, 423-437, 1976.

Alexandrov, T., and Golyandina, N.: The automatic extraction of time series trend and periodical components with the help of the Caterpillar-SSA approach, Exponenta Pro, 3, 54-61, 2004.

Bakhmutov, V., and Groza, A.: The dilatancy-diffusion model: new prospects, Proceedings, International Conference: Problems of Geocosmos, 7th, St. Petersburg, Russia, May, 2008, 26-30.

Bhattacharya, P. M., Mukhopadhyay, S., Majumdar, R., and Kayal, J.: 3-D seismic structure of the northeast India region and its implications for local and regional tectonics, Journal of Asian Earth Sciences, 33, 25-41, 2008.

Bhattacharya, P. M., Kayal, J., Baruah, S., and Arefiev, S.: Earthquake source zones in northeast India: seismic tomography, fractal dimension and b value mapping, in: Seismogenesis and Earthquake Forecasting: The Frank Evison Volume II, Springer, 145-158, 2010.

Chetia, T., Baruah, S., Dey, C., Sharma, S., and Baruah, S.: Multi-parametric approach for Earthquake Precursor Detection in Assam Valley (Eastern Himalaya, India) using Satellite and Ground Observation Data, Geotectonics, In Press, 2019.

Chetia, T., Baruah, S., Dey, C., Sharma, S., and Baruah, S.: Probabilistic analysis of seismic data for earthquake forecast in North-East India and its vicinity, Current Science, In Press, 2019.

Choubey, V., Kumar, N., and Arora, B.: Precursory signatures in the radon and geohydrological borehole data for M4. 9 Kharsali earthquake of Garhwal Himalaya, Science of the total environment, 407, 5877-5883, 2009.

Demmel, J., and Veselić, K.: Jacobi's method is more accurate than QR, SIAM Journal on Matrix Analysis and Applications, 13, 1204-1245, 1992.

Fraedrich, K.: Estimating the dimensions of weather and climate attractors, Journal of the atmospheric sciences, 43, 419-432, 1986.

Golyandina, N., Nekrutkin, V., and Solntsev, V.: „Caterpillar"-SSA Technique for Analysis of Time Series in Economics, New Models of Business: Managerial Aspects and Enabling Technology, 198, 2001.

Golyandina, N., Nekrutkin, V., and Zhigljavsky, A. A.: Analysis of time series structure: SSA and related techniques, Chapman and Hall/CRC, 2001.

Golyandina, N.: On the choice of parameters in singular spectrum analysis and related subspace-based methods, arXiv preprint arXiv:1005.4374, 2010.

Gupta, H.: Medium-term earthquake prediction, Eos, Transactions American Geophysical Union, 69, 1620-1630, 1988.

401 Gutenberg, B., and Richter, C. F.: Frequency of earthquakes in California, Bulletin of the
402 Seismological society of America, 34, 185-188, 1944.

403 Gutenberg, B.: The energy of earthquakes, Quarterly Journal of the Geological Society, 112,
404 1-14, 1956.

405 Hartmann, J., and Levy, J. K.: Hydrogeological and gasgeochemical earthquake precursors–A
406 review for application, Natural Hazards, 34, 279-304, 2005.

407 Hassani, H.: Singular spectrum analysis: methodology and comparison, 2007.

408 Kayal, J., Arefiev, S., Barua, S., Hazarika, D., Gogoi, N., Kumar, A., Chowdhury, S., and
409 Kalita, S.: Shillong plateau earthquakes in northeast India region: complex tectonic
410 model, CURRENT SCIENCE-BANGALORE-, 91, 109, 2006.

411 Kayal, J.: Microearthquake seismology and seismotectonics of South Asia, Springer Science
412 & Business Media, 2008.

413 Kayal, J., Arefiev, S. S., Baruah, S., Tatevossian, R., Gogoi, N., Sanoujam, M., Gautam, J.,
414 Hazarika, D., and Borah, D.: The 2009 Bhutan and Assam felt earthquakes (Mw 6.3
415 and 5.1) at the Kopili fault in the northeast Himalaya region, Geomatics, Natural
416 Hazards and Risk, 1, 273-281, 2010.

417 Kayal, J., Arefiev, S., Baruah, S., Hazarika, D., Gogoi, N., Gautam, J., Baruah, S., Dorbath, C.,
418 and Tatevossian, R.: Large and great earthquakes in the Shillong plateau–Assam valley
419 area of Northeast India Region: Pop-up and transverse tectonics, Tectonophysics, 532,
420 186-192, 2012.

421 Khan, M. A. R., and Poskitt, D.: Window length selection and signal-noise separation and
422 reconstruction in singular spectrum analysis, Monash Econometrics and Business
423 Statistics Working Papers, 23, 2011-2023, 2011.

424 Khattri, K., and Tyagi, A.: Seismicity patterns in the Himalayan plate boundary and
425 identification of the areas of high seismic potential, Tectonophysics, 96, 281-297, 1983.

426 Kumar, A., Walia, V., Arora, B. R., Yang, T. F., Lin, S.-J., Fu, C.-C., Chen, C.-H., and Wen,
427 K.-L.: Identifications and removal of diurnal and semidiurnal variations in radon time
428 series data of Hsinhua monitoring station in SW Taiwan using singular spectrum
429 analysis, Natural Hazards, 79, 317-330, 2015.

430 Merolla, P., Mose, D., and King, A.: Effect of water table fluctuations on radon emanation
431 from soil, 2003.

432 Miklavčić, I., Radolić, V., Vuković, B., Poje, M., Varga, M., Stanić, D., and Planinić, J.: Radon
433 anomaly in soil gas as an earthquake precursor, Applied radiation and isotopes, 66,
434 1459-1466, 2008.

435 Nandy, D., and Dasgupta, S.: Seismotectonic domains of northeastern India and adjacent areas,
436 Physics and Chemistry of the Earth, 18, 371-384, 1991.

437 Nandy, D.: Geodynamics of Northeastern India and the adjoining region, ACB publications,
438 2001.

439 Ni, J., and Barazangi, M.: Seismotectonics of the Himalayan collision zone: Geometry of the
440 underthrusting Indian plate beneath the Himalaya, Journal of Geophysical Research:
441 Solid Earth, 89, 1147-1163, 1984.

442 Nielson, K., Rogers, V., and Gee, G.: Diffusion of Radon through Soils: A Pore Distribution
443 Model 1, Soil Science Society of America Journal, 48, 482-487, 1984.

444 Reasenberg, P.: Second-order moment of central California seismicity, 1969–1982, Journal of
445 Geophysical Research: Solid Earth, 90, 5479-5495, 1985.

446 Serita, A., Hattori, K., Yoshino, C., Hayakawa, M., and Isezaki, N.: Principal component
447 analysis and singular spectrum analysis of ULF geomagnetic data associated with
448 earthquakes, Natural Hazards and Earth System Science, 5, 685-689, 2005.

449 Sharma, A. K., Walia, V., and Virk, H.: Effect of meteorological parameters on radon
450 emanation at Palampur (HP), Journal of Association of Exploration Geophysicists, 21,
451 47-50, 2000.

452 Singh, S., Kumar, A., Bajwa, B. S., Mahajan, S., Kumar, V., and Dhar, S.: Radon monitoring
453 in soil gas and ground water for earthquake prediction studies in North West Himalayas,
454 India, Terr. Atmos. Ocean. Sci, 21, 685-695, 2010.

455 Stranden, E., Kolstad, A., and Lind, B.: The influence of moisture and temperature on radon
456 exhalation, Radiation Protection Dosimetry, 7, 55-58, 1984.

457 Tomer, A.: Radon as a earthquake precursor: a review, Int J Sci Eng Technol, 4, 815-822, 2016.

458 Ulomov, V., and Mavashev, B.: The Tashkent Earthquake of 26 April, Tashkent: Acad. Nauk.
459 Uzbeck, 1971.

460 Verma, M., and Bansal, B. K.: Earthquake precursory studies in India: Scenario and future
461 perspectives, Journal of Asian Earth Sciences, 54, 1-8, 2012.

462 Virk, H., and Singh, B.: Radon recording of Uttarkashi earthquake, Geophysical Research
463 Letters, 21, 737-740, 1994.

464 Walia, V., Su, T., Fu, C., and Yang, T.: Spatial variations of radon and helium concentrations
465 in soil-gas across the Shan-Chiao fault, Northern Taiwan, Radiation Measurements, 40,
466 513-516, 2005.

467 Wiemer, S.: A software package to analyze seismicity: ZMAP, Seismological Research Letters,
468 72, 373-382, 2001.

469 Yang, T., Walia, V., Chyi, L., Fu, C., Chen, C.-H., Liu, T., Song, S., Lee, C., and Lee, M.:
470 Variations of soil radon and thoron concentrations in a fault zone and prospective
471 earthquakes in SW Taiwan, Radiation Measurements, 40, 496-502, 2005.

472

473

474

475

476 **FIGURES AND TABLES**

477

478

479

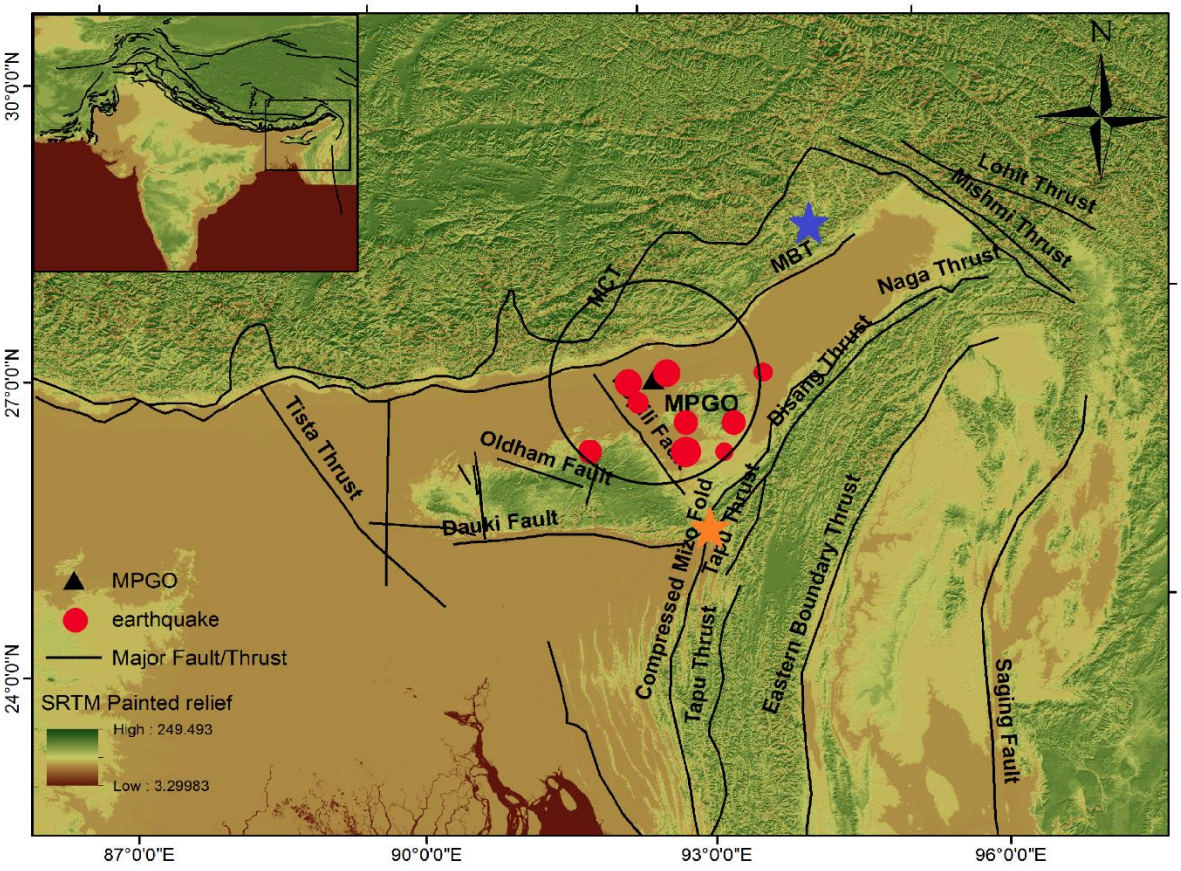

480

481 **Figure 1:** Map illustrates the main tectonic features of North-East (after Kayal, 2006), India
482 along with the study area represented by black color circle and the earthquake events (3.1 ≤ mb
483 ≤ 3.7) which were found to have correlation with soil radon emanation anomalies are
484 represented by the red color dots. The black color triangle represents the Multiparametric
485 Geophysical Observatory. The blue color star represents the earthquake of Mw~7.2, 1947 and
486 orange color star represents the earthquake of Mw~7.7, 1869.

487

488

489

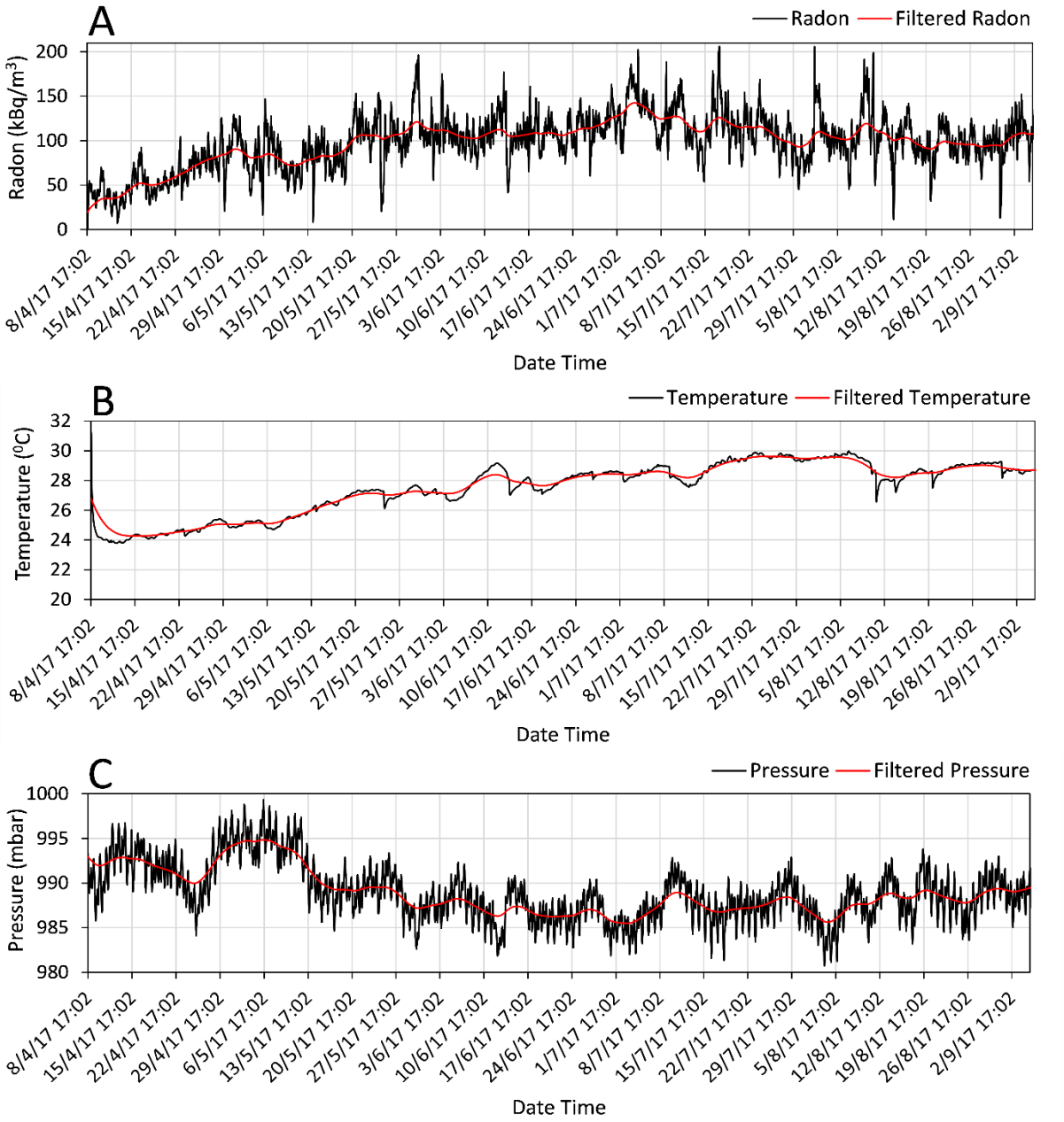

490

491 **Figure 2:** The plot represents the removal of high frequency quasi periodic component for A)
492 filtered time series of soil radon, B) filtered time series of soil temperature and C) filtered time
493 series of soil pressure.

494

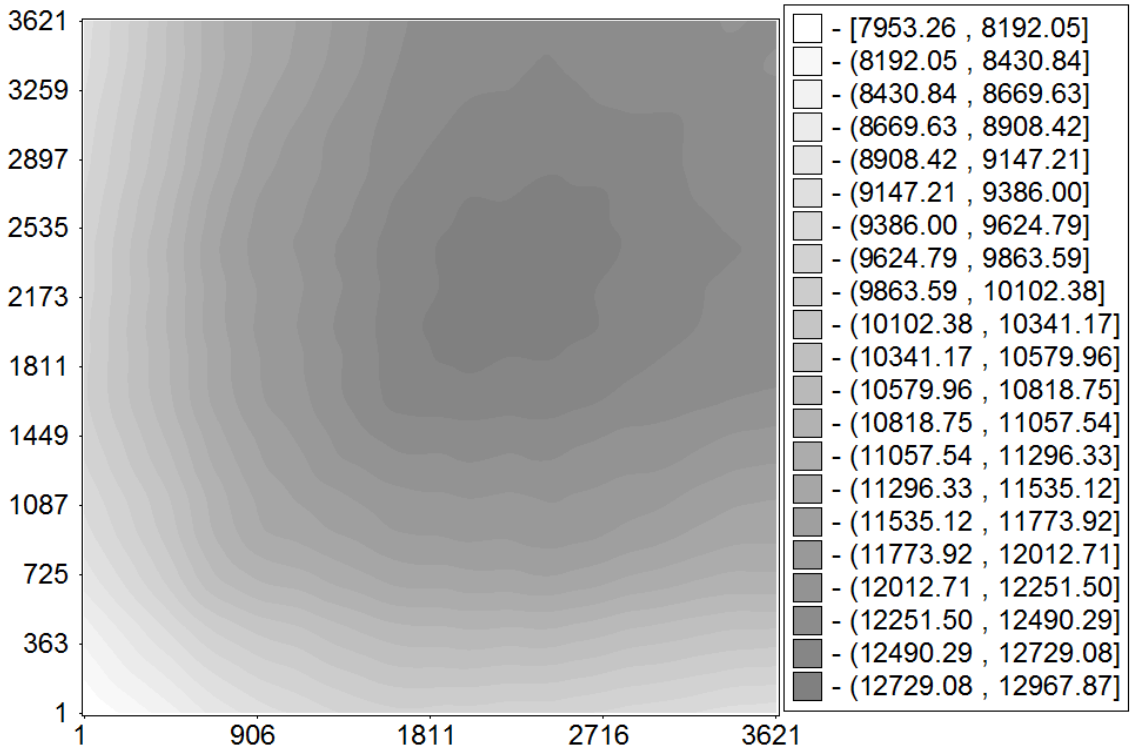

Figure 3: Covariance matrix of the first 9 group of soil radon (Rn-222) time series.

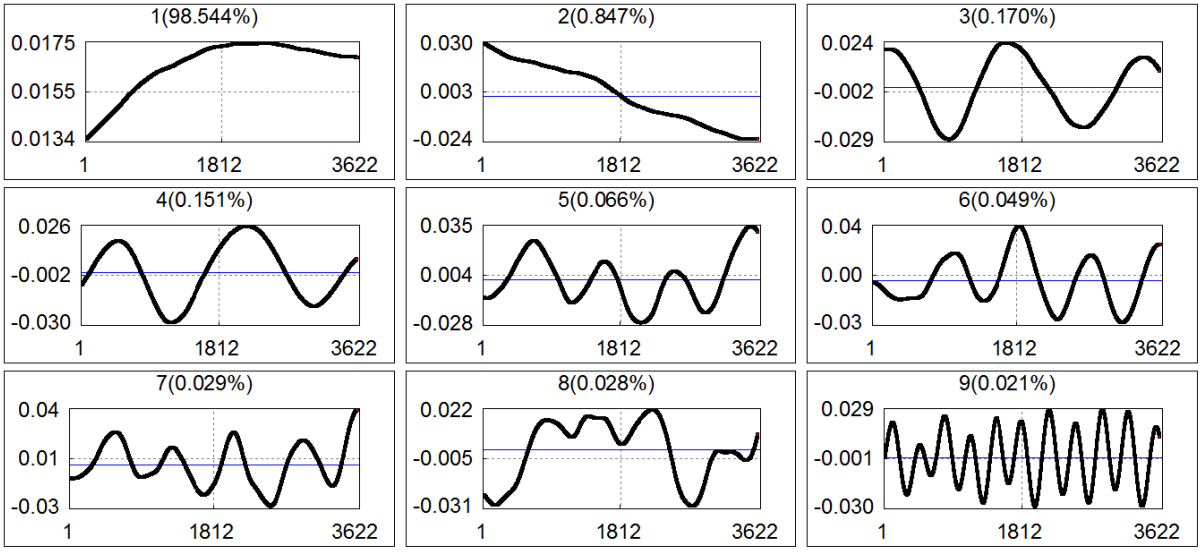

Figure 4: Eigenfunctions of soil radon (Rn-222) first 9 group. The scale in the horizontal x-axis represents the window length (L*15 minutes) and the scale in the vertical y-axis represents the singular eigenvectors (matrix path SVD).

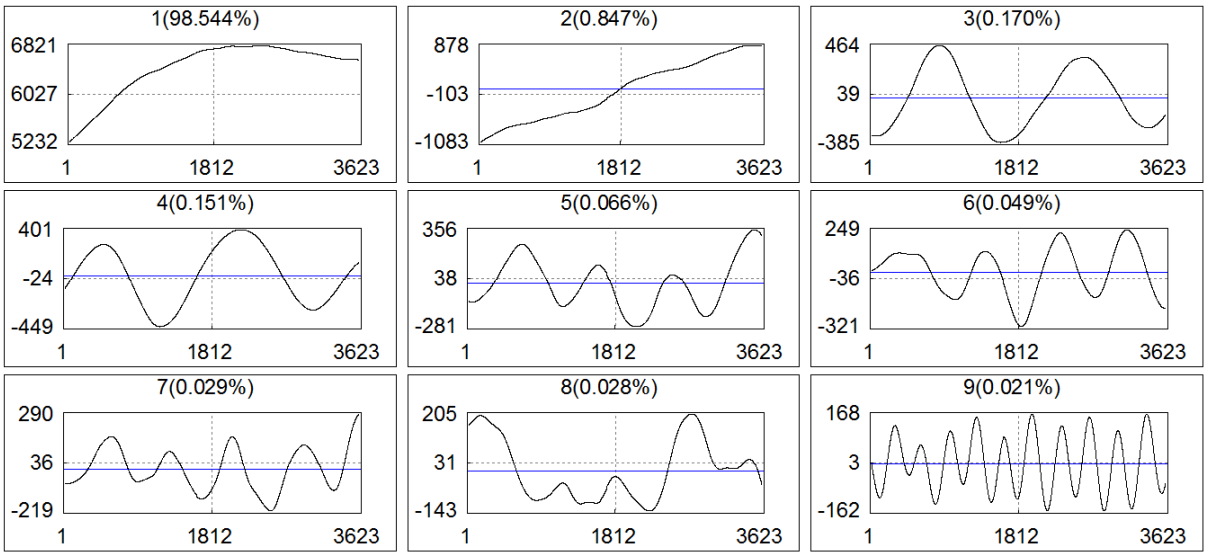

Figure 5: Principal Component of soil radon (Rn-222) related to the first 9 eigentriples. The scale in the horizontal x-axis represents the window length (L*15 minutes) and the scale in vertical y-axis represents the Principal Component (PC).

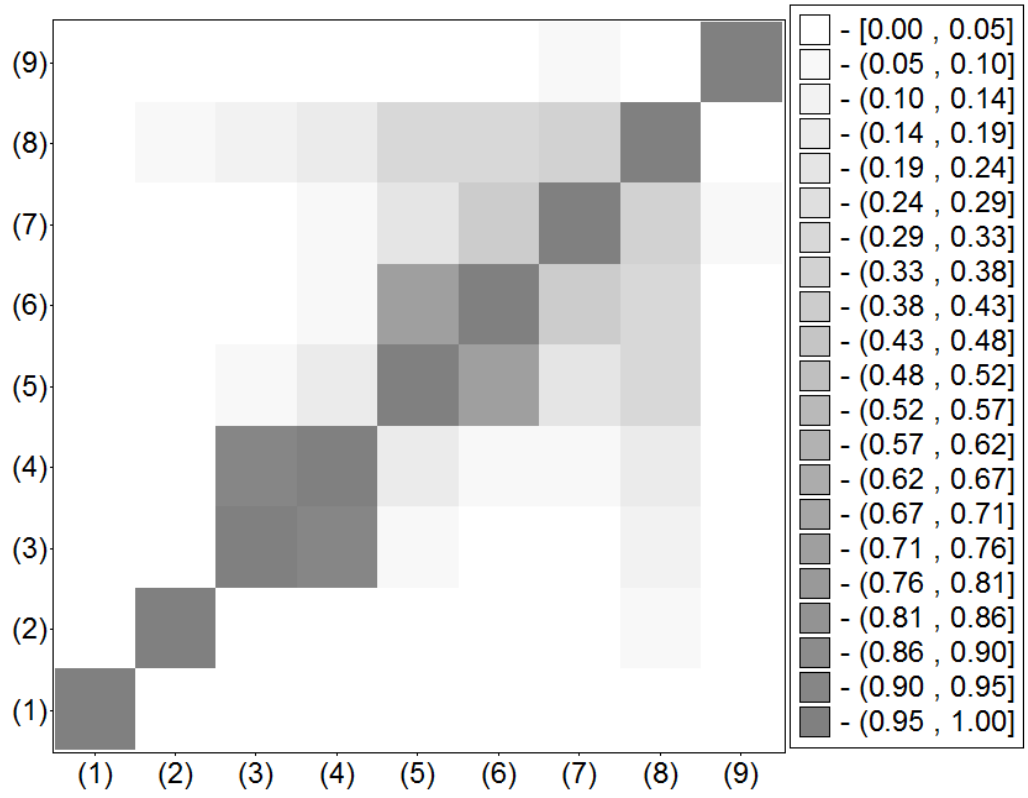

Figure 6: w-correlation matrix for the 9 reconstructed components of soil radon time series.

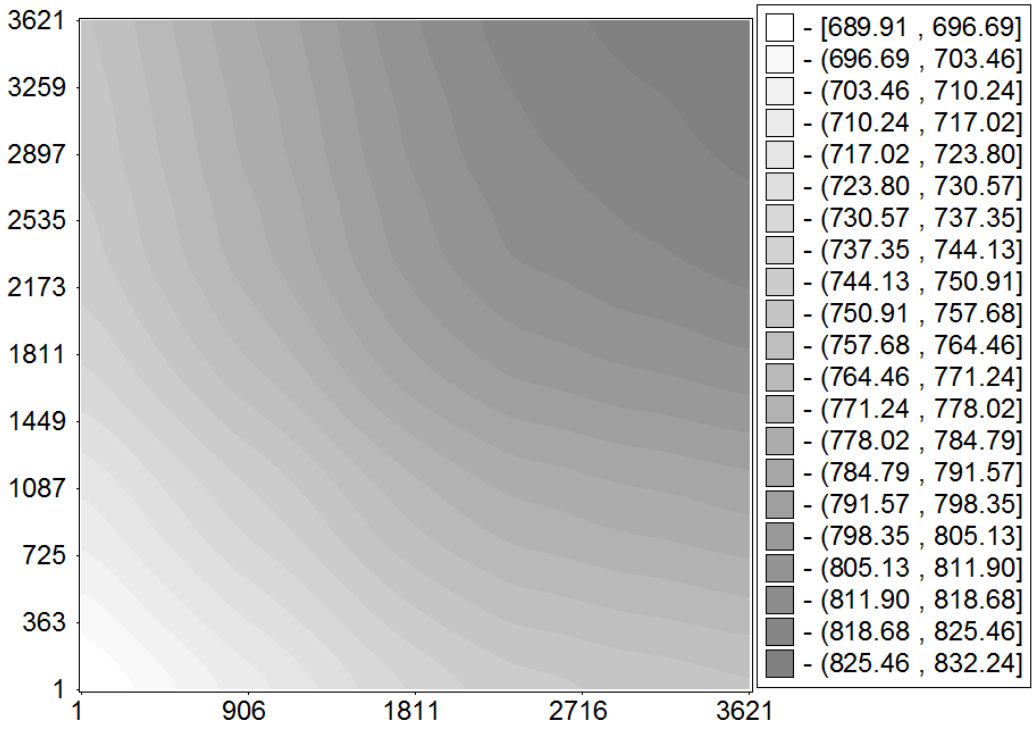

509

510 **Figure 7:** Covariance matrix of the first 9 group of soil temperature time series.

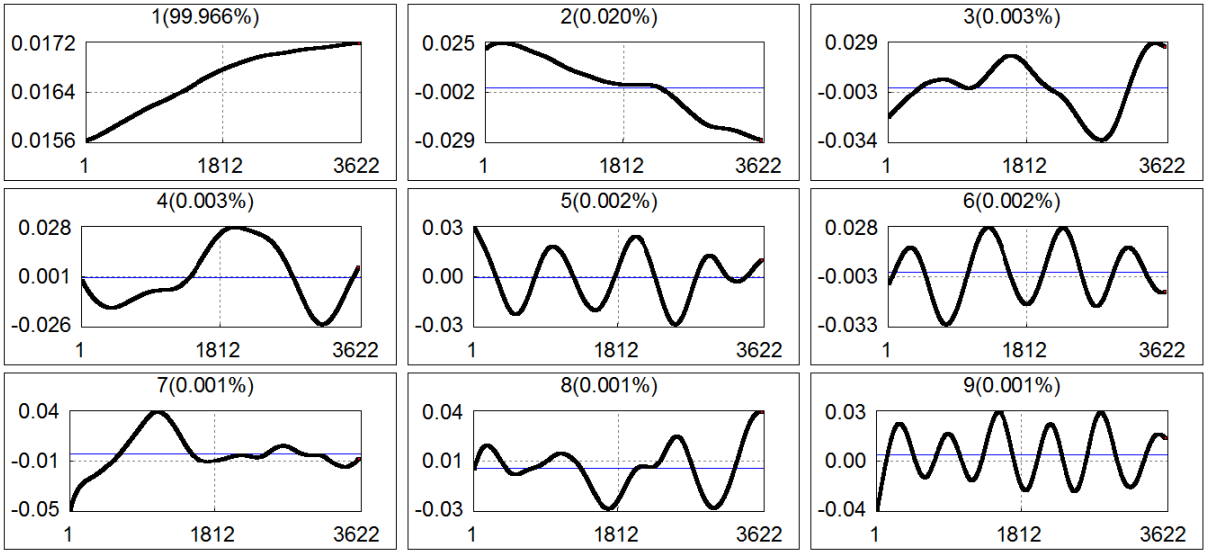

511

512 **Figure 8:** Eigenfunctions of soil temperature first 9 group. The scale in the horizontal x-axis

513 represents the window length (L*15 minutes) and the scale in the vertical y-axis represents the

514 singular eigenvectors (matrix path SVD).

515

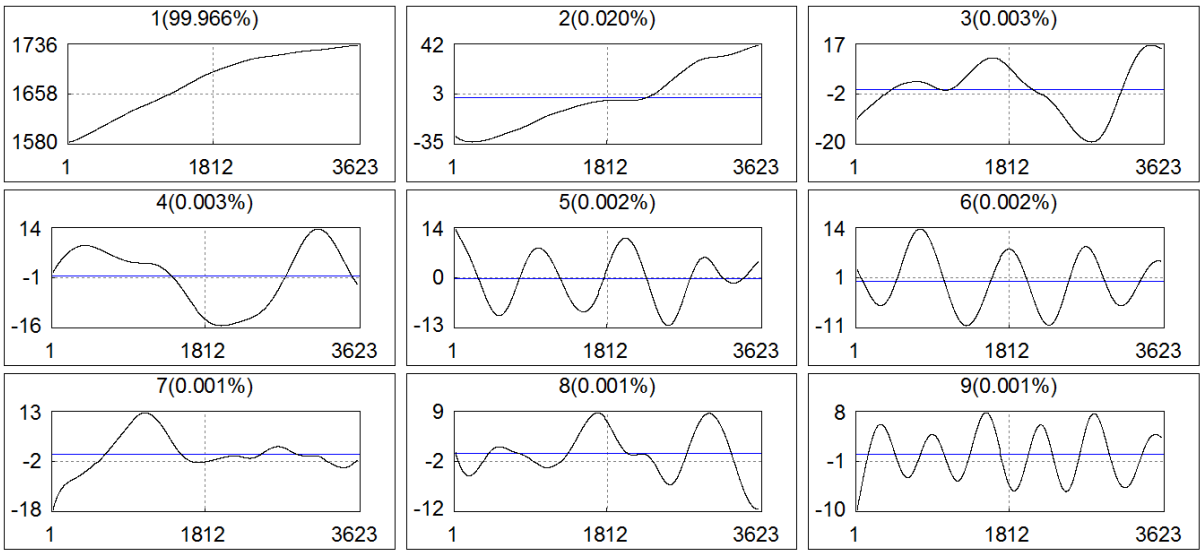

Figure 9: Principal Component of soil temperature related to the first 9 eigentriples. The scale in the horizontal x-axis represents the window length (L*15 minutes) and the scale in the vertical y-axis represents the Principal Component (PC).

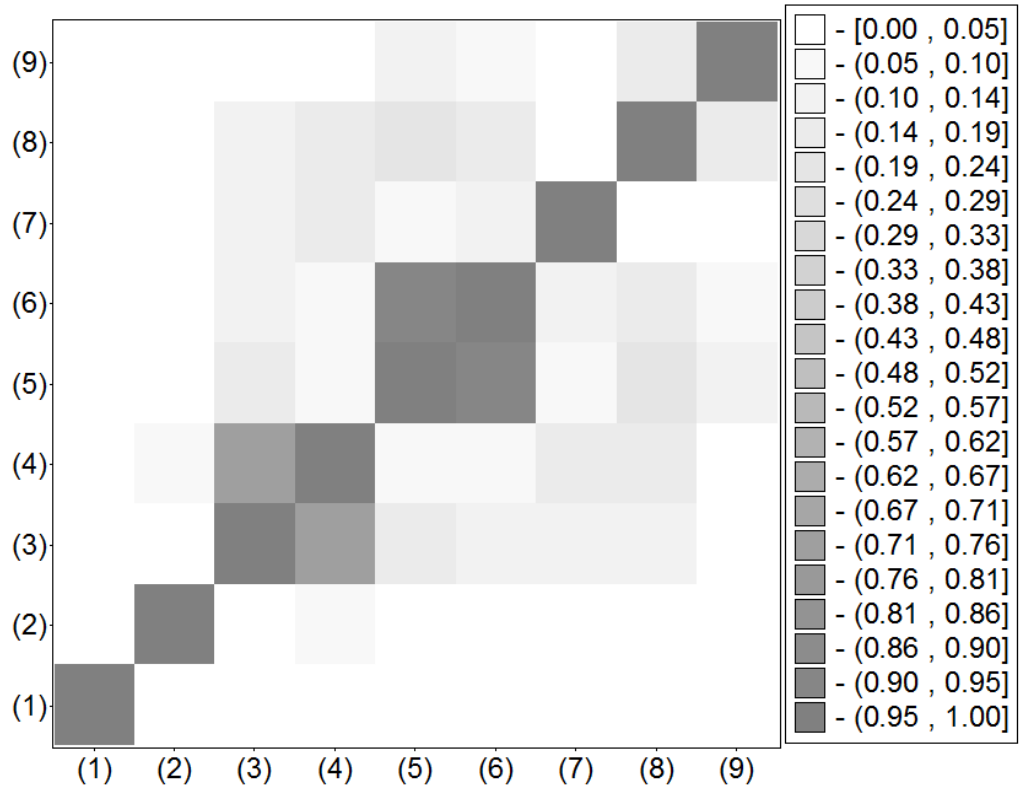

Figure 10: w-Correlation matrix for the 9 reconstructed components of soil temperature time series.

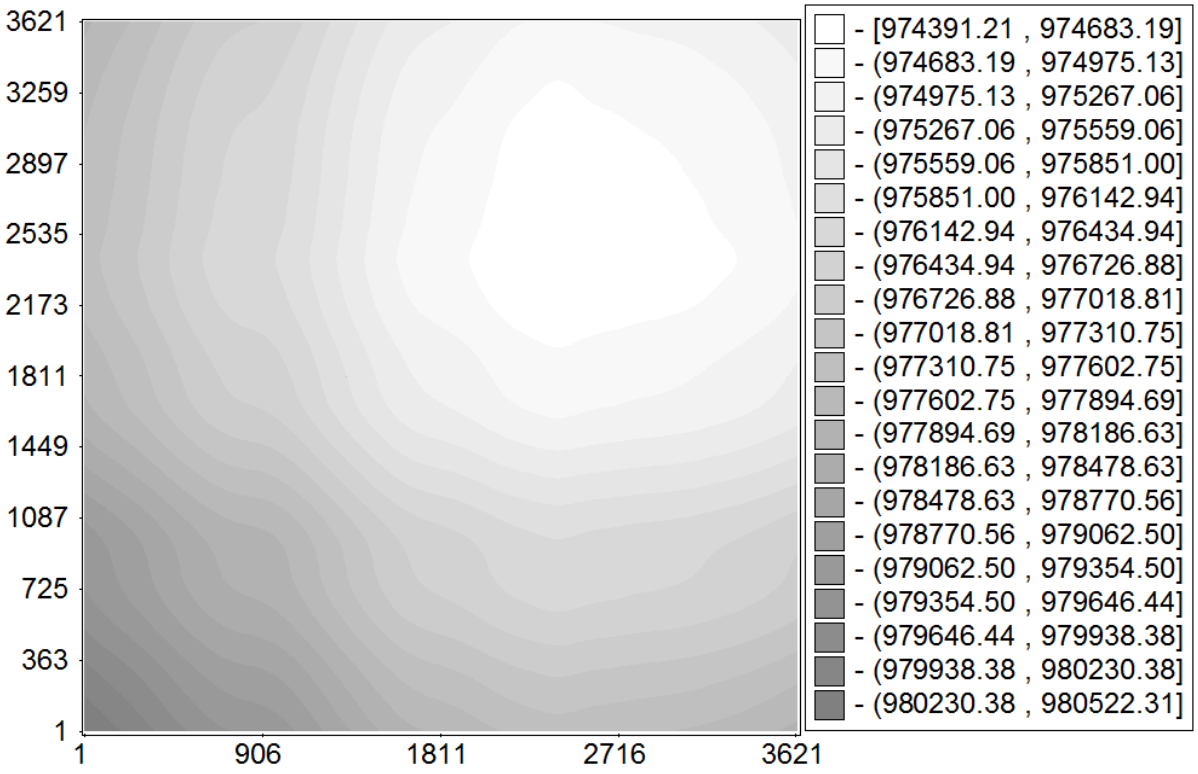

Figure 11: Covariance matrix of the first 9 group of soil pressure time series

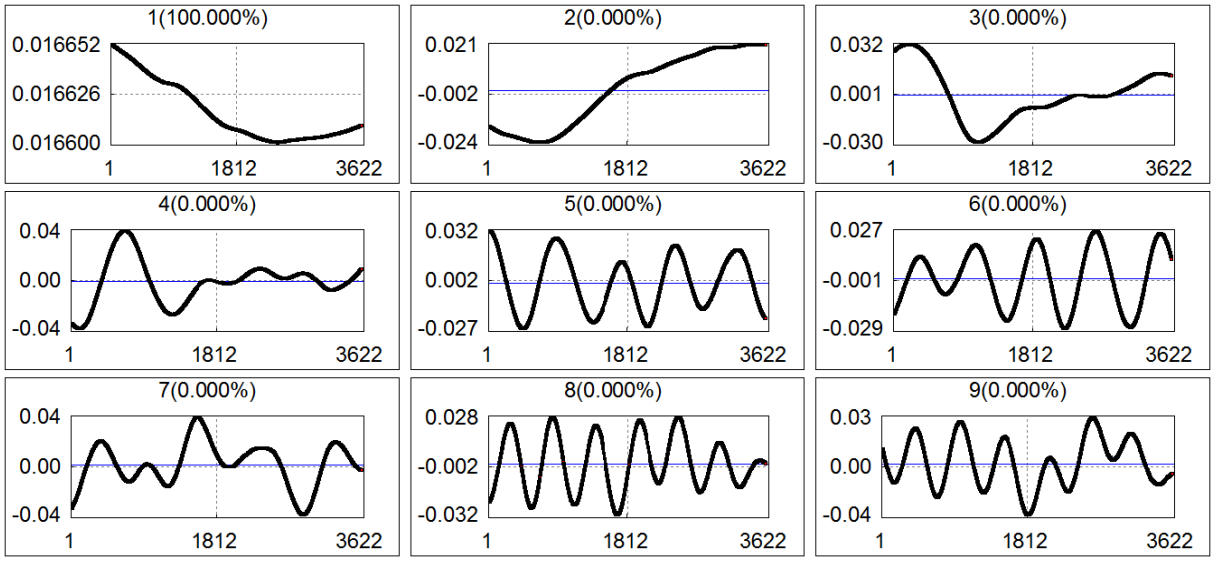

Figure 12: Eigenfunctions of soil pressure first 9 group. The scale in the horizontal x-axis represents the window length (L*15 minutes) and the scale in the vertical y-axis represents the singular eigenvectors (matrix path SVD). .

530

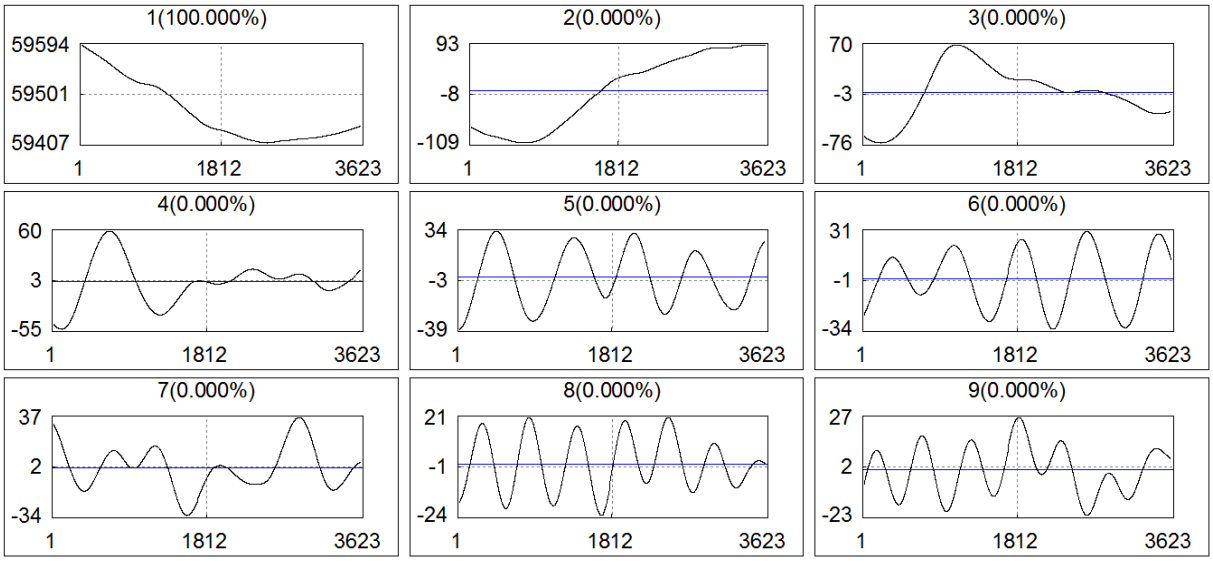

531

532 **Figure 13:** Principal Component of soil temperature related to the first 9 Eigentriples. The
533 scale in the horizontal x-axis represents the window length (*L**15 minutes) and scale in the
534 vertical y-axis represents the Principal Component (PC).

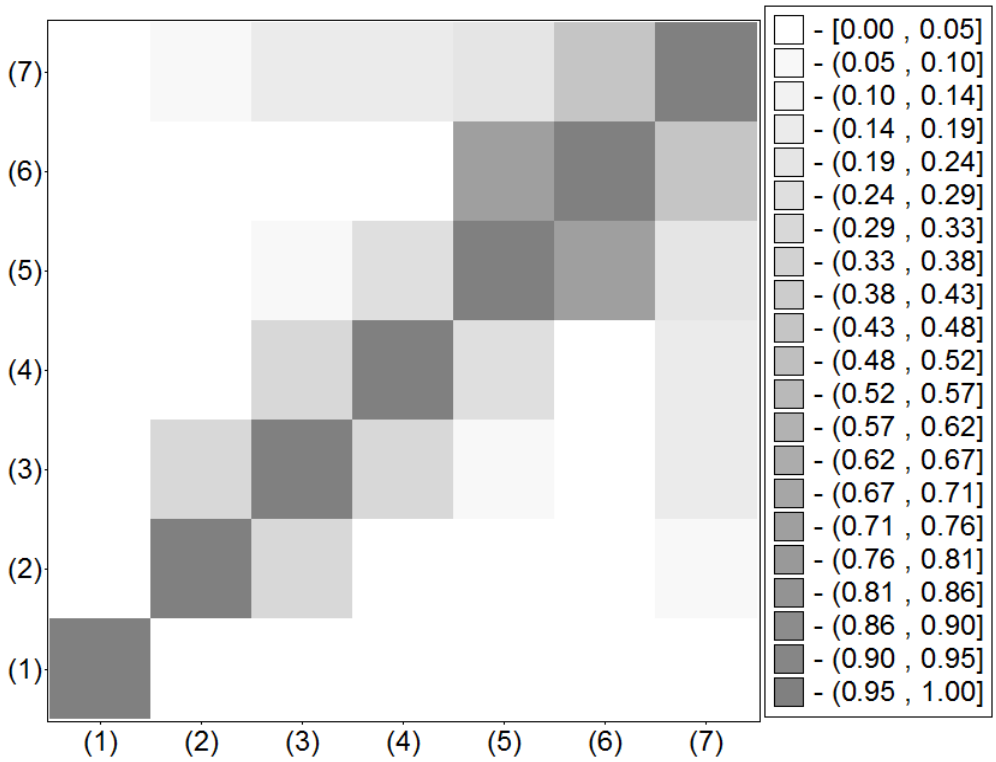

535

536 Figure 14: w correlation matrix for the 9 reconstructed components of soil pressure time series.

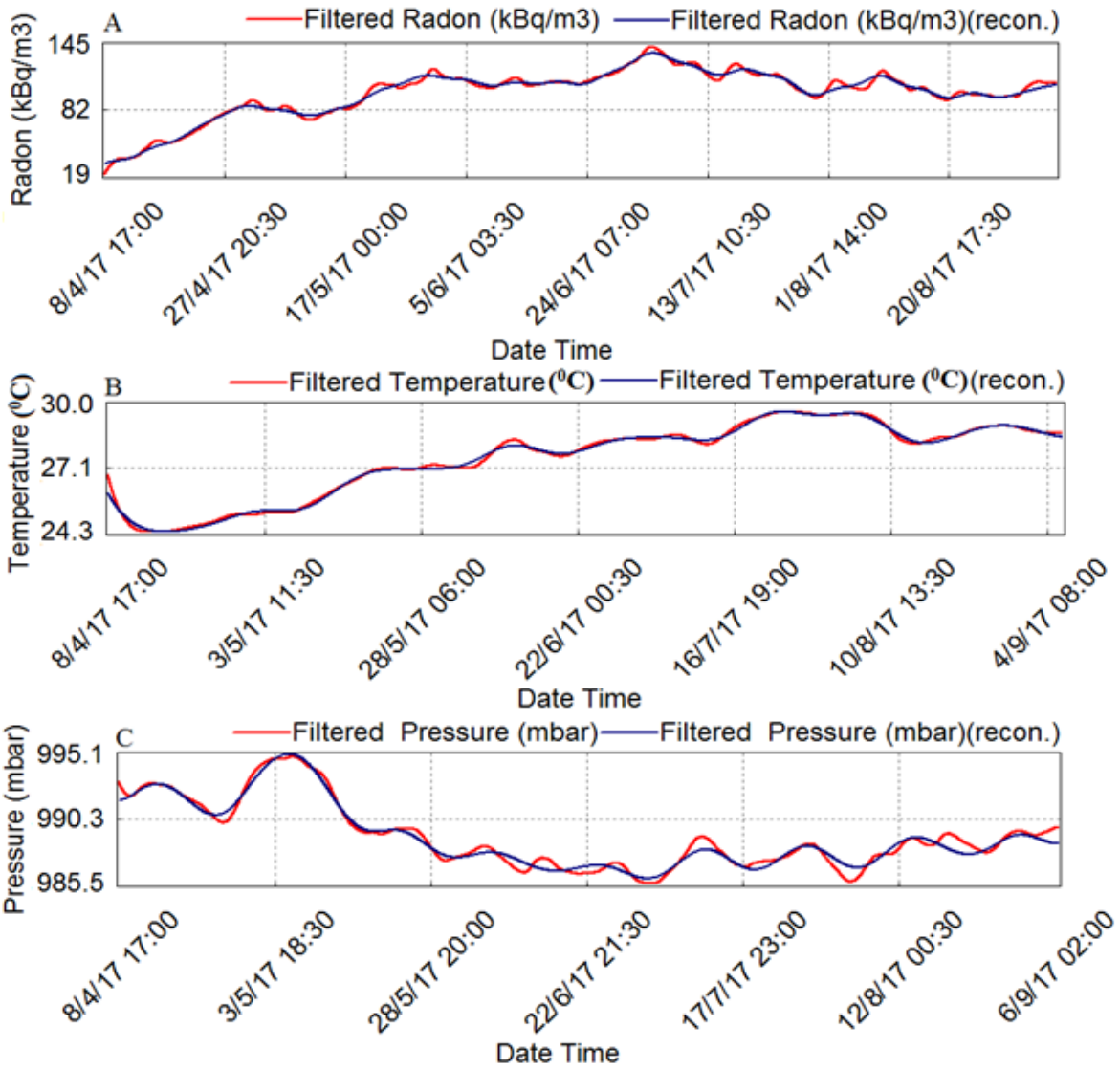

Figure 15: Plot showing the reconstructed time series of A) filtered soil radon, B) filtered temperature and C) filtered pressure.

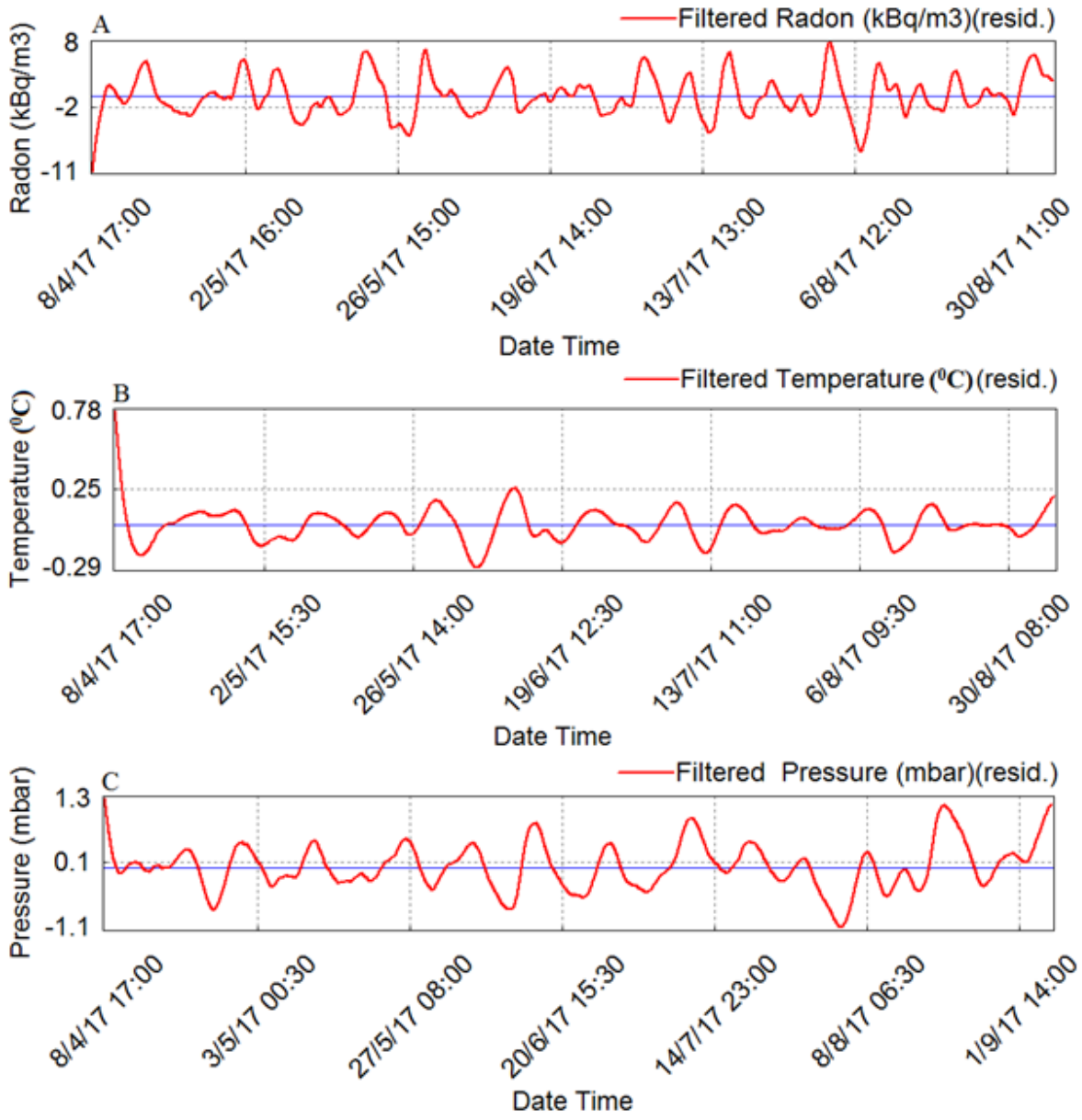

545

546 **Figure 16:** Residual of reconstructed time series of A) Filtered soil radon, B) temperature and

547 C) pressure respectively.

548

549

550

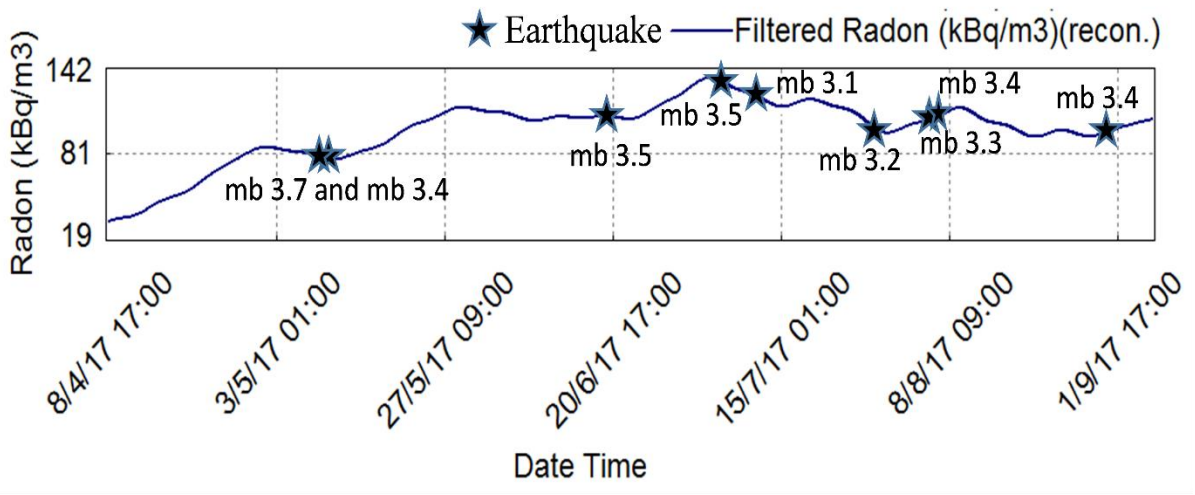

551

552 **Figure 17:** Plot showing the reconstructed filtered time series of soil radon emanation along
553 with earthquake during the investigation period in the vicinity of MPGO, Tezpur (~100 km
554 radially from MPGO) which occurred in a very short span of time.

555

556

557

558

559

560

561

562

563

564

565 **Table 1:** The average emanation of soil-gas radon and the standard deviation at MPGO from
566 April to September, 2017.

Month (2017)	Average Rn-222 emanation (kBq /m3)	Standard Deviation (kBq /m3)
April	55.94	21.3
May	93.11	28.53
June	109.12	19.07
July	117.69	28.09
August	101.45	25.86
September	92.34	18.65

567

568

569 **Table 2:** The correlation co-efficient of soil radon gas concentration with soil pressure and
570 temperature at OH-MPGO during year 2017.

Parameters	Average (Avg.)	Standard Deviation (Std.)	Coefficient of Variation (Std./Avg. %)	Correlation Coefficient
Radon (KBq/m^3)	94.94	23.58	24.84	----
Temperature (^0C)	28.60	0.62	2.19	0.51
Pressure (mbar)	991.03	2.48	0.25	-0.52

571

572

573

574 **Table 3:** Hypocentral parameters of the earthquake events found to have correlation with radon
575 anomaly.

Date of Event	UTC TIME	Lat (°N)	Long (°E)	Place	Depth (km)	Mag (m_b)	Distance from MPGO (km)	Type of Anomaly (+ or -)
9/5/17	01:53:55	26.3	92.7	Assam	25	3.7	44	+
9/5/17	03:26:54	26.6	93.2	Assam	28	3.4	67	+
20/6/17	04:31:58	27.1	92.5	West Kameng, Arunachal Pradesh	10	3.5	67	+
4/7/17	10:05:47	27.0	92.1	West Kameng, Arunachal Pradesh	10	3.5	78	-
10/7/17	23:28:30	27.1	93.8	Papumpare, Arunachal Pradesh	10	3.1	78	-
25/7/17	18:28:00	26.3	93.1	Karbi Anglong, Assam	28	3.2	67	-
5/8/17	12:24:56	26.8	92.2	Darrang, Assam	10	3.3	44	+
7/8/17	11:25:07	26.3	91.7	Kamrup, Assam	10	3.4	100	+
31/8/17	17:57:26	26.6	92.7	Sonitpur Assam	10	3.4	67	+

576
577
578
579
580
581